Fluid Dynamics of a Bistable Diverter Under Ultrasonic Excitation - Part I: Performance Characteristic

Michael Mair

PhD Student
Oxford Thermofluids Institute
Department of Engineering Science
University of Oxford
OX2 0ES Oxford, United Kingdom

Marko Bacic

University Research Lecturer
Oxford Thermofluids Institute
Department of Engineering Science
University of Oxford
OX2 0ES Oxford, United Kingdom
Email: marko.bacic@eng.ox.ac.uk

ABSTRACT

This paper investigates an ultrasonically driven bistable fluidic diverter at inlet nozzle Mach numbers of up to $Mn = 0.3$ and operating pressure ratios of up to $Pr = 1.1$. Part I examines the switching characteristics with respect to non-dimensional parameters of excitation amplitude, frequency, required energy, switching time and inlet total pressure. It is shown that to promote switching at turbulent jet Mach numbers of up to $Mn = 0.3$ it is necessary to excite a jet preferred mode of St=0.45 which differs from previously reported laminar jet operation of the similar device. For the reference case the switching time amounts to $1.2\,ms$ suggesting oscillation frequencies of up to $800\,Hz$. Part II is a combined experimental and numerical study that examines the triggered

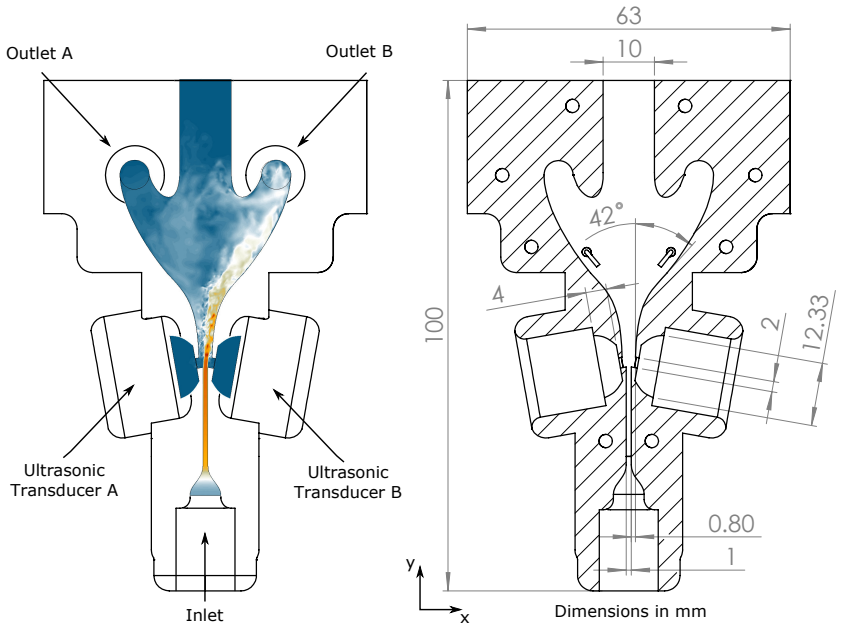

Fig. 1: Left: Basic device layout and an example snapshot of a LES simulation showing attachment on side B. Right: Schematic and governing dimensions of the fluidic device in mm

instability modes in the free shear layer using Large Eddy Simulations (LES) and visualises the flow field using Particle Image Velocimetry (PIV).

1 INTRODUCTION

Step changes in the performance of aerospace and automotive components cannot be expected by pure passive shape design. Flow control, in contrast, holds the potential to unlock significant efficiency gains and fuel burn improvements by manipulating or suppressing undesired flow phenomena. Over the last two decades this has led to a renaissance in flow control research focusing on both passive and active methods. The variety of applications and concepts is vast and includes boundary layer separation control [1–7], drag reduction of ground vehicles [8–10], unsteady film cooling [11, 12], combustion instability control [13], jet vectoring [14], mixing enhancements [15, 16], cavity tone and resonance suppression [17, 18] as well as the control of secondary flow phenomena in inlet ducts or highly loaded compressors and turbines [19–23]. The enormous amount of published articles regarding different strategies and applications demonstrate not only the huge interest within the aerospace community but also the difficulties and challenges that still

persist. As a result, flow control devices are still rarely seen in real world applications and commercial progress has mainly been hampered by the lack of reliable, low weight and high bandwidth actuators. We are presenting a novel no-moving parts fluidic switching device for active flow control that due to its ability to switch realistic (0.3 Mn) jets offers hope for higher TRL development and eventual industrial application in aerospace (Fig.1).

In general, fluidic devices convert a continuous inflow into an oscillating or sweeping outflow using either active or passive means. Passive fluidic oscillators have received by far the most attention in the past. This is mainly due to their relative simplicity and robustness since they rely entirely on fluid instabilities or internal feedback channels [24–26]. A comprehensive review of passive fluidic oscillators can be found in [27] or [28]. However, an inherent limitation of passive oscillators is that the output oscillation frequency depends on the device geometry as well as on the mass flow rate and thus somehow restricts the bandwidth of the device. For a high bandwidth variable-frequency oscillator that can also be phase-locked to the flow phenomena in question, e.g. rotating stall or fan flutter, an active mechanism is required. Such flow control devices are bistable in nature and take advantage of the Coanda effect, the tendency of a jet of fluid to be attached to an adjacent wall. If the device is supplied with a pressurized fluid, a jet of air issues from the nozzle orifice and encounters a highly unstable region in which any small disturbance produces a pressure gradient across the jet [29]. When such a gradient is developed, the main flow bends towards one surface or the other and once this imbalance is developed, the fluid adheres to the wall by means of the Coanda effect. If no control is applied, the attachment remains stable and the flow follows the surface of the wall. If a small amount of force/momentum is exerted at the right location, the flow detaches and switches to the opposite wall. The challenge here is the development of a suitable actuation mechanism that imposes the force necessary to switch the jet. An excellent review of existing flow control actuators including purely fluidic, moving surface and plasma actuators can be found in [30].

During the early years of oscillator development transverse blowing or air extraction was the most common technique to drive the de- and reattachment process [31, 32]. This, however, calls for additional air supply systems including valves or flaps which in turn feature a relatively long

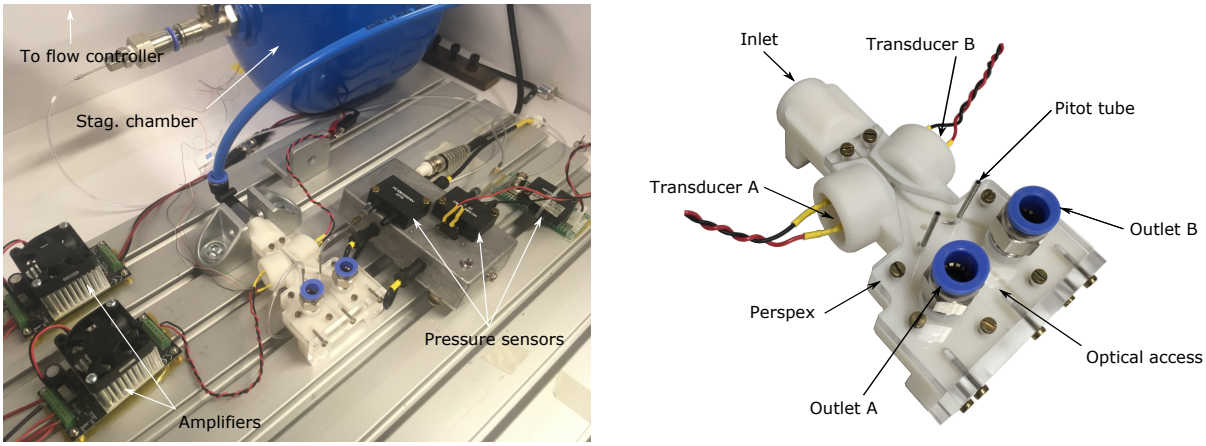

Fig. 2: Schematic of the experimental set-up

response time as well as a higher propensity to mechanical damage. This has spurred more recent studies to focus on novel switching mechanisms that exclude secondary air systems. Gregory et al. [33], for instance, used a cantilever piezoelectric beam located on the jet centreline with its free end oscillating up and down at the nozzle orifice (nozzle width w = 0.5 mm). The device was capable of switching high-speed jets (Mn = 1) up to a frequency of 5 Hz. The concept successfully decouples the frequency from the prevalent flow rate and is able to operate at engine realistic pressure ratios. Both Gregory et al. [34] and Tesař et al. [35] used Single Dielectric Barrier Discharge (SDBD) actuators inside control port channels and the interaction region, respectively, but only achieved switching at low flow velocities. More recently, Martin et al. [36] used a piezoelectric driven synthetic jet actuator to switch a bistable fluid diverter with main jet velocities up to $5\,\frac{m}{s}$. Chen et al. [37] used a spark discharge inside the recirculation bubble to switch the flow. The device was successfully operated at pressure ratios up to 1.1 ($u_e = 50\,\frac{m}{s}$ and $Re = 10000$).

The present study describes a novel actively controlled fluidic oscillator concept that is based on the acoustic excitation of natural instabilities in the ultrasonic range. A proof of concept study was published previously which showed that if an initially laminar jet is excited at its shear layer mode ($St_\theta = 0.012$) an increased entrainment on the unattached side leads to a pressure drop sufficient to counteract the initial attachment force [38]. Here we extend the operational bandwidth of the device to engine realistic pressure ratios and velocities of up to $Mn = 0.3$.

Section 2 discusses the experimental set-up as well as its respective uncertainties. Section 3

highlights the governing design aspects of acoustically driven FSDs and shows how the relatively small wavelengths of ultrasonic frequencies can be used to amplify the sound pressure level. Experimental results in section 4 determine the switching characteristics subject to changes in pressure ratio, excitation properties and density. The dynamic performance of the device is further shown as well. Section 5 finally concludes the paper.

2 EXPERIMENTAL METHODOLOGY

2.1 Experimental Set-up

The present FSD is supplied with pressurized fluid via an Omega FMA-2609A flow controller. A stagnation chamber just upstream of the device inlet is used to measure the total to static pressure ratio Pr (HCX002D6V). The device is 3D printed, features a perspex cover plate to allow flow visualization studies and has a weight of less than $150g$ (see Fig.1&2). Pitot probes on both attachment sides are attached to customary pressure transducers (HCXM350D6V) to record the total gauge pressure at $f_s = 30\,kHz$. The data is further filtered using an analog low pass filter with a cut off frequency at $1.5\,kHz$. The tube length between Pitot probe and pressure transducer is kept below 50mm so that the response time of the tubing exceeds the cut off frequency by a factor of 2 and its length has no adverse effect on the measured data. The switching time is then defined as the time between the onset of excitation and the point where the signal exceeds 90% of the final mean value. Both outlets can be connected to a single needle valve to increase the back pressure and thus allow experiments at higher densities. 250ST150 Prowave ultrasonic transducers with a resonance frequency at $25\,kHz$ are mounted inside both control port chambers (see Fig3). The square wave signal is provided by two Tektronix AFG1022 signal generators and amplified using an ultra-low noise amplifier (PDu150). The sound pressure level is recorded downstream of the nozzle orifice with a high intensity omnidirectional Kulite microphone at $f_s = 250\,kHz$ (Mic-093). Each data point presented in this paper is averaged using ten successive switching events. The minimum required acoustic energy to enable switching is defined as

$$E = \int_0^{t_{ex}} P(t)dt = \frac{Ap^2}{\rho c} \cdot cos\theta \cdot t_{ex} \tag{1}$$

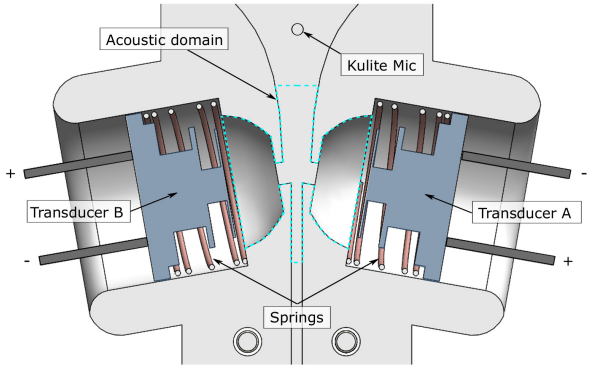

Fig. 3: Cutaway model of the nozzle and interaction region and display of the acoustic domain

where t_{ex} is the minimum excitation time that switches the jet 10 out of 10 times. Flow conditions are turbulent through out the study ($Re_h = 6000\,to\,13000$ based on nozzle height h).

2.2 Experimental Uncertainties

Pressure measurements of the Pitot probes feature an uncertainty that is more than two orders of magnitude lower than the average variation in switching time and therefore negligible. The pressure ratio $Pr = \frac{p_{t,in}}{p_{s,out}}$ determined by the total pressure inside the stagnation chamber exhibits an uncertainty of $\pm 1\%$. The set mass flow rates feature an uncertainty of 2% but are corrected in hindsight using an orifice plate leading to an uncertainty of less than $\pm 1\%$. All dimensions of the 3D printed device are measured separately to check for possible discrepancies. Deviations from the design point amount to less than $0.1\,mm$ (10% of h) but are included in all subsequent calculations. The sound pressure level measured inside the interaction region is accurate to within $\pm 0.3\%$. The experimental set-up is further described in Fig.2.

3 FLUIDIC DESIGN

3.1 Fluidic Jet Behaviour

Typical bistable devices have two independent outlet channels that are separated by a splitter. The location of such a splitter is usually crucial to the performance of the device. For an upstream location close to the nozzle orifice, for instance, the jet attachment will become unstable as soon as the splitter leading edge interacts with the jet potential core. Furthermore, the location of the

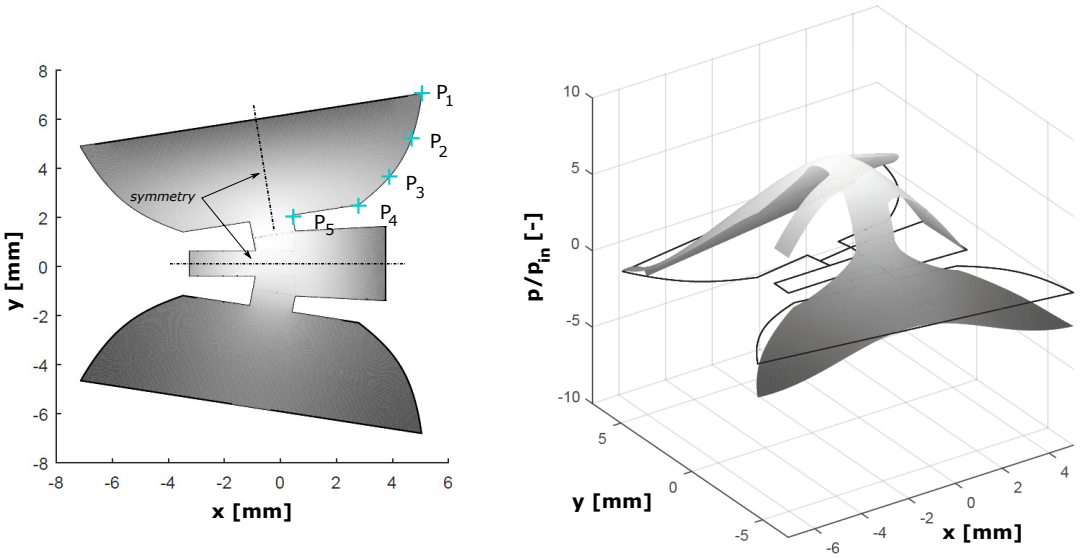

(a) Left: Acoustic domain with 5 Bezier points and symmetry lines, right: input pressure amplification of the optimized design across the domain

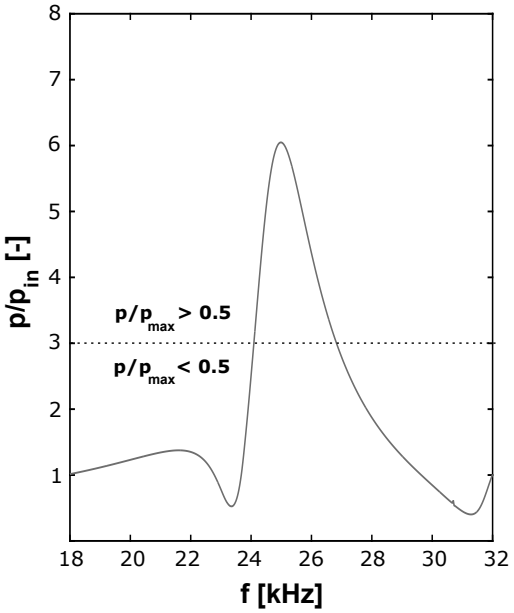

(b) Amplification of input pressure vs. frequency with full width at half maximum

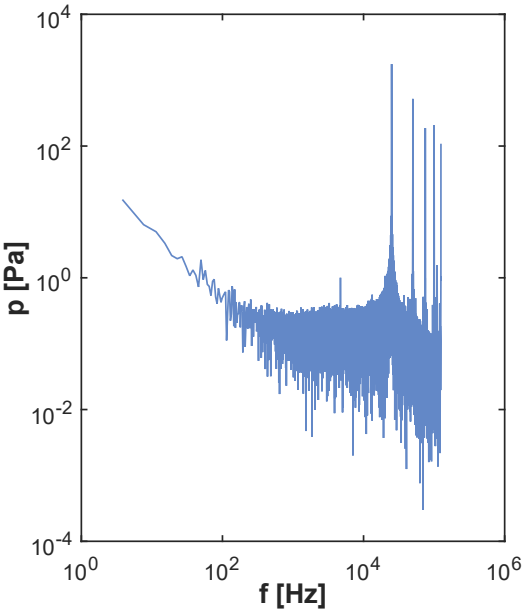

(c) Frequency response measured by Kulite microphone at $f_{ex} = 25\,kHz$ and maximum input voltage

Fig. 4: Acoustic optimisation of the control port chamber

leading edge also determines where the reverse mass flow, if present, is fed into the main jet and therefore might strengthen the attachment. While some switching mechanisms require the presence of a splitter, such as the plasma switched vortex valve in [37], acoustic excitation works

just as fine without. The enhanced entrainment and subsequent pressure drop on the unattached side due to excitation is independent of a splitter being present or not. The reason for the present FSD not having such a splitter is twofold. First, it enables non-intrusive laser optical measurements (PIV) which will be discussed in Part II of this study and second, it demonstrates the ability to operate the device as a frequency controlled sweeping jet.

Other governing geometric parameters of bistable devices are set-back distance and wall attachment angle. For acoustically driven devices, it is especially the set-back distance that enables the switching in the first place. A too large set-back would allow that the enhanced entrainment is supplied by an infinite reservoir, e.g. reverse mass flow, and the rolled-up vortical structures would not form a confined space with the attachment wall. Hence the pressure would not drop and switching would not occur. It is therefore obvious to correlate the set-back distance to the size of the expected vortical structures. This means that the set-back should not be larger than the nozzle height itself. The present FSD features a set-back of $0.8h$ as it was used in a previous study. Set-backs smaller than that have only limited effect on the pressure drop of the unattached side since the volume from which fluid is entrained depends mainly on the size of the control port chamber.

The attachment wall angle has an effect on the curvature of the jet centreline and therefore the strength of the attachment force. Here, a straight attachment wall for the first two nozzle heights downstream of the orifice and a subsequent increase to 40° with respect to the streamwise direction is used. The attachment was found to be remarkably stable and is maintained even if the outlet is completely blocked. The aspect ratio is $AR = \frac{w}{h} = 3$.

3.2 Non-dimensional Parameters

Based on the results gained in [38] the dominant parameters that determine the switching characteristics are the sound amplitude $\hat{p}$, the excitation frequency f, the required energy E, the pressure ratio Pr, the density ρ, the jet speed u_e, the distance L between a possible splitter and the nozzle orifice, the nozzle height h and finally the momentum thickness of the unattached shear

layer θ. The switching time can thus be written as:

$$t_s = f(\hat{p}, f, E, Pr, \rho, u_e, L, h, \theta) \tag{2}$$

This can be transformed into:

$$\frac{t_s u_e}{L} = f(\frac{\hat{p}}{\rho u_e^2}, \frac{fh}{u_e}, \frac{E}{u_e^2 \rho h^3}, Pr, \frac{L}{h}, \frac{h}{\theta}) \tag{3}$$

or rather

$$T_s = f(Am, St_h, \bar{E}, Pr, \frac{L}{h}, \frac{h}{\theta}). \tag{4}$$

The switching time is non-dimensionalised by the transport time, the time it takes a fluid particle to travel form the nozzle orifice to the splitter leading edge assuming a constant velocity u_e. For the splitterless configuration considered subsequently the splitter distance L is replaced by the distance between the nozzle and the Pitot probe.

The first parameter on the right of Eq.4 is the non-dimensional pressure amplitude which we will call the Amplitude Flow Factor Am. It indicates that the sound power required for switching scales with the kinetic energy of the flow. The second parameter, the Strouhal number St, can either be based on the nozzle height h or the momentum thickness θ. Subsequently St_h, or rather $St_{D_{eq}}$ is used since it offers a better comparison with other published articles that use circular nozzles. The non-dimensional energy $\bar{E}$ is a pure function of the excitation time if signal properties and flow conditions remain the same. Together with the pressure ratio Pr and the switching time T_s, those three parameters form the foundation of all subsequent performance characteristics.

The two remaining parameters $\frac{L}{h}$ and $\frac{h}{\theta}$ are independent of the excitation properties but nonetheless affect the switching process. $\frac{L}{h}$ is a dominant geometric parameter that, as already

outlined, can considerably alter the flow field itself. Depending on the actuation mechanism as well as on the shape of the splitter, values for $\frac{L}{h}$ are typically between 5 and 12 [25, 39]. The ratio of nozzle height to momentum thickness, equivalent to $\frac{Re_h}{Re_\theta}$, is an important parameter with significant contribution to the downstream development of vortices. In [38] it was shown that for an initially laminar jet, hence small $\frac{h}{\theta}$, the only mode at which switching is feasible corresponds to the shear layer roll-up frequency at $St_\theta = 0.012$. Excitation of the natural instability of a laminar jet shifts the roll-up location and therefore the entrainment of ambient fluid to further upstream positions. The forced entrainment closer to the nozzle orifice counteracts the attachment force and triggers the switching. However, as the Reynolds number and the ratio of nozzle height to momentum thickness increases the location of the natural roll-up advances towards the nozzle orifice even without any forcing present. With respect to an acoustically driven FSD, this means that a sufficient increase in entrainment (which counteracts the attachment force) is unlikely to be accomplished by fundamental forcing if Re exceeds a certain threshold. In other words, the excitation and amplification of the primary instability ($St_\theta = 0.012$) will not achieve the necessary increase in entrainment if $\frac{h}{\theta}$ is high since the shear layer characteristics become less dependent on the initial roll-up of vortical structures. This suggests that different instability modes, e.g. sub-harmonic or jet preferred mode, need to be addressed if Re exceeds a certain threshold. Clearly, this threshold corresponds to the location of the shear layer roll-up and hence to $\frac{h}{\theta}$. The ratio of nozzle height to momentum thickness can therefore be used as a measure for which instability has to be excited and, what will be shown later, which length scale the non-dimensional frequency St should be based on.

3.3 Acoustic Considerations

A big advantage of using ultrasonic frequencies is that the wavelength of the acoustic signal becomes comparable to the dimensions of the device ($\lambda_{25kHz} \approx 10h$). This means that the control port chamber can be used to amplify the sound pressure level by matching one of its eigenmodes to the transducer resonance frequency. Such eigenmodes can be found by means of the Helmholtz equation, a time-independent form of the wave equation as described in Chapter 3. Solving the wave equation in the frequency domain then yields the frequency response at any given point for a

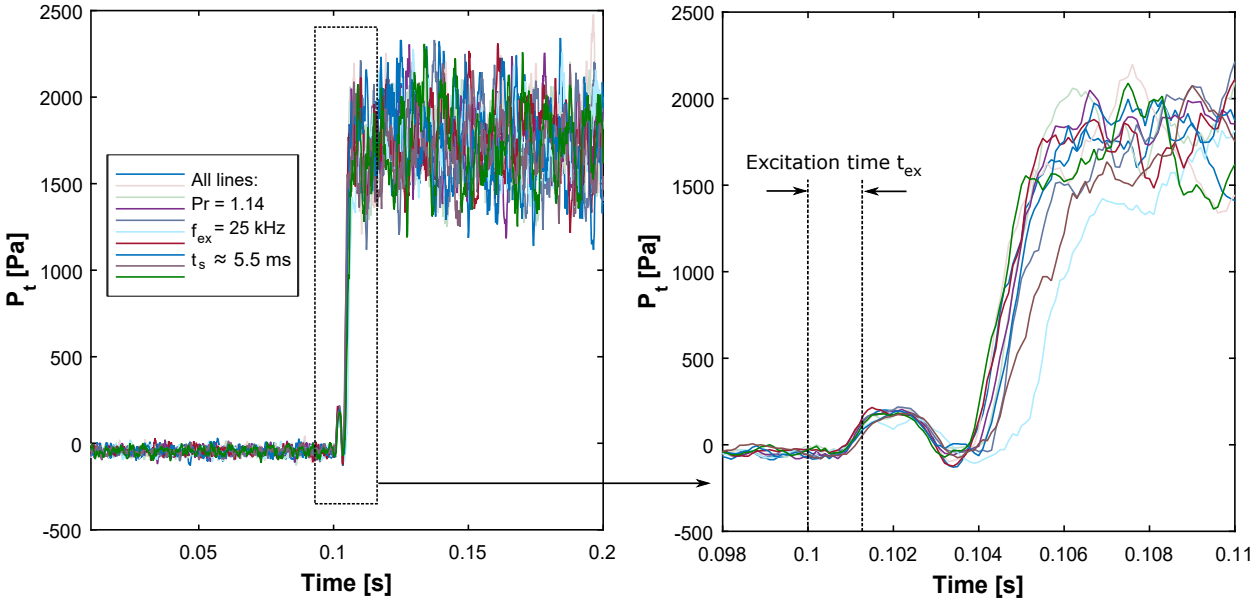

Fig. 5: Ten successive switching events measured via the Pitot probe (for location of probe see Fig.1) and close-up view for the comparison of different time scales

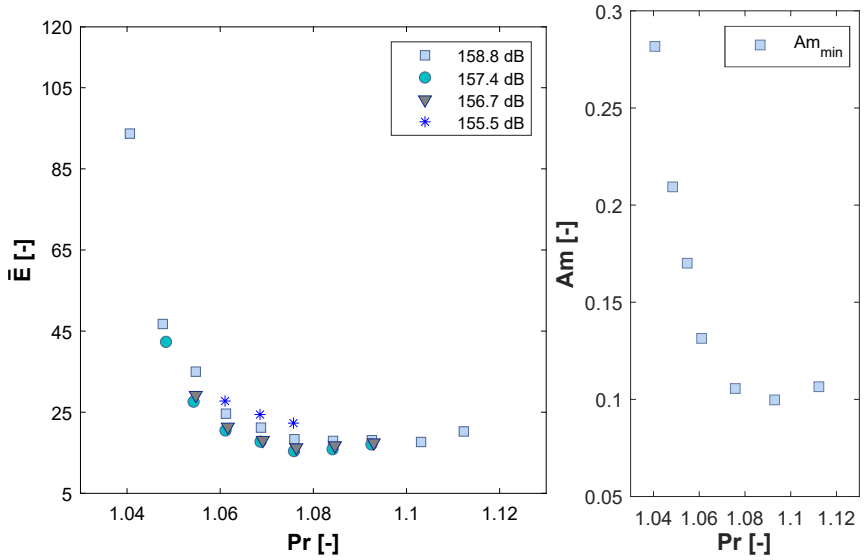

(a) Minimum required energy

(b) Minimum required Amplitude Flow factor

Fig. 6: Non-dimensional switching parameters as a function of Pr

given geometry. With regard to the present FSD this means that the control port chamber should have a geometry that satisfies the requirements of sufficient amplification of the input signal so to enable switching. Such a geometry can be found by iteratively solving the time-independent wave

equation along with an optimisation algorithm. Here a simple gradient based algorithm that uses the so called interior-point method is used [?]. The objectives for the design are

1 Keep chamber resonant frequency close to transducer resonant frequency

2 Maximise sound pressure level SPL at resonant frequency

3 Design for Q so that bandwidth is $2\,kHz$

Note that the latter objective takes into account inevitable manufacturing tolerances. The objectives can be summarized mathematically as

$$f(x) = min \begin{cases} |f_T - f^*| \\ \frac{1}{SPL^*} \\ |\frac{f_T}{2\,kHz} - Q| \end{cases} \tag{5}$$

f_T is the transducer resonance frequency and f^* the frequency at the highest sound pressure level SPL^*. The location where SPL^* is computed is a separate measurement domain between the control port throat and the nozzle orifice, the point where the acoustic wave interacts with the shear layer. The variables to be optimized are the x and y coordinates of 5 Bézier points that form each side wall of the symmetrical control port chambers. The acoustic domain in which the wave equation is solved for frequencies between $18 - 32\,kHz$ is further highlighted in Fig.3 and Fig.4 a.). Given that the optimisation requires more than 100 iterations it is further opted for a 2D eigenmode calculation to keep computational costs within reasonable bounds. The optimised geometry, as shown in Fig.3, features a sextuple amplification of the input pressure (Fig.4 b.)). In absolute numbers this amounts to a maximum sound pressure level of $158.8\,dB$ for the splitterless configuration (Fig.4 c.)).

Furthermore, Tam [40] derived a measure of the relative sensitivity of the shear layer to sound induced instability as a function of the angle of incidence. For the range of Mach numbers expected in this study ($Mn \approx 0.3$) the angle that generates instability waves with the largest amplitudes was found to be 10°. The control port chambers are thus rotated by 10° with respect to the cross-stream y-direction. Fig.3 further shows that springs are used to place the ultrasonic transducers inside

the chambers. This was found to ensure that the membrane is at the correct location so to obtain the amplification set by the optimisation.

4 RESULTS

4.1 Performance Characteristic

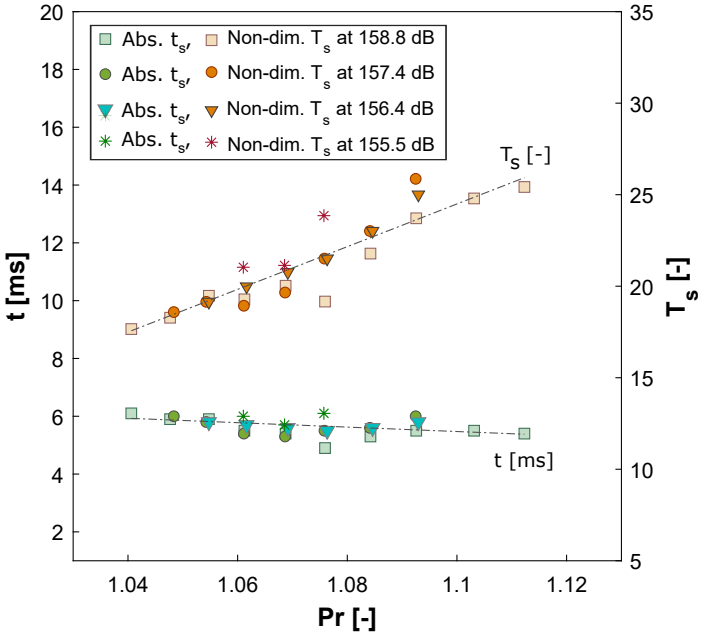

Fig. 7: Non-dimensional and absolute switching time vs. Strouhal number and pressure ratio for different sound pressure levels

4.1.1 Switching Characteristics

Fig.5 shows an example for 10 successive switching events at $Pr = 1.07$ ($Mn \approx 0.3$) measured via the Pitot probe on the initially unattached side. The average switching time amounts to $t_s = 5.5\,ms$ with a maximum deviation of 9%. The negative total gauge pressure measured on the unattached side illustrates the reverse mass flow that supplies the entrainment of the unforced jet. The graph further reveals that the excitation time, defined as the number of excitation cycles divided by the frequency, is only a fraction of the time needed to switch the jet, that all lines show a similar hump prior to the switching and that the actual switching seems somehow delayed. Note

that the delay is an order of magnitude larger than the transport time and is therefore not caused by the downstream location of the Pitot probe. The short excitation time indicates that the driving force, caused by the pressure drop on the unattached side, is reached long before the jet has fully responded to the new steady state condition. This indicates that the jet has already attached to the opposite side after the excitation has stopped but the recirculation bubble on the initial attachment side persists, increases in size and elongates downstream (see Fig.8). This 'double attached' flow

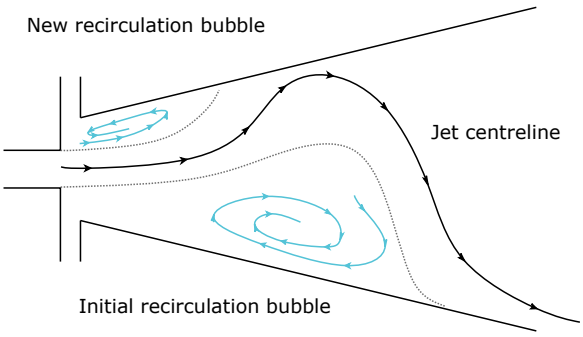

Fig. 8: Schematic of a 'double attached' flow

stalls the detachment from the initial side and causes the delay in switching. This again is simply due to the absence of a splitter that would otherwise prevent the elongation of the recirculation bubble. It is interesting to note that the condition of the 'double attachment' persists for several flow-through times. However, it is reasonable to assume that the switching time can be decreased by either using a splitter or introducing vents downstream of the reattachment point.

The hump, which is consistent for every single switching event, shows that the shear layer responds instantly with an increased spreading rate as of the onset of excitation. The deflected shear layer travels downstream along the attachment wall and is measured as an increase in total pressure ($10ms$ after the onset of excitation). This is verified by the fact that the hump starts off one flow-through time between the nozzle and the Pitot probe after the onset of excitation and that the flat peak of the hump lasts exactly for t_{ex}.

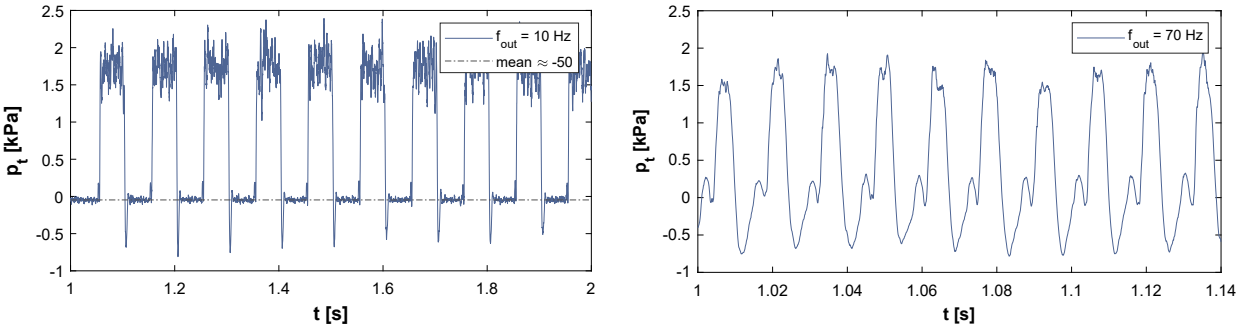

(a) $f_{out} = 10\,Hz$ (b) $f_{out} = 70\,Hz$

Fig. 9: Dynamic switching at two different oscillation frequencies

4.1.2 Non-dimensional Energy and Switching Time

It was found in the previous section that the minimum required energy to switch the jet serves as an appropriate criterion to find the preferred pressure ratio and/or Strouhal number for a fixed excitation frequency. In that respect Fig.6 a.) shows the non-dimensional minimum energy for four different sound pressure levels as a function of Pr. An increase in sound pressure level simply increases the range of pressure ratios that enable switching similar to the results at laminar flow conditions and low frequency excitation presented in [38]. At the lowest sound pressure level switching is only feasible between $Pr = 1.06$ and $Pr = 1.075$, or rather $St_{D_{eq}} = 0.47$ and $St_{D_{eq}} = 0.43$. The preferred pressure ratio ($Pr \approx 1.07$) thus seems to be at $St_{D_{eq}} \approx 0.45$ suggesting that the excitation of the jet preferred mode is responsible for switching [41]. The non-dimensional energy exhibits an exponential increase as the pressure ratio approaches the lower end ($Pr = 1.04$) at which only the highest tested amplitude ($\hat{p} = 158.8\,dB$) can switch the jet. At higher pressure ratios, in contrast, only a moderate linear increase in $\bar{E}$ is required for switching. The global minimum in energy ($\bar{E}$) is found around $Pr = 1.075$ which corresponds to $St_{D_{eq}} = 0.43$ and is marginally shifted to higher pressure ratios with respect to the preferred mode. In absolute terms the energy E follows a symmetrical parabolic curve with its minimum at $St_{D_{eq}} = 0.45$ ($Pr = 1.07$). The shift towards higher pressure ratios when looked at the non-dimensional numbers is also shown in Fig.6. Here the minimum required non-dimensional amplitude Am corresponds to $Pr \approx 1.09$. It is clear that the minimum amplitude that allows switching increases exponentially as the pressure ratio moves away from the preferred mode. This can be observed especially at lower pressure

ratios since $Am \propto \frac{1}{u_c^2}$. The minimum required amplitude flow factor around the jet preferred mode amounts to ≈ 0.1. The absolute power required to switch the jet varies between 10 and $200mW$.

The non-dimensional switching time, shown in Fig.7, exhibits a linear increase over Pr that results in a minor decrease when put to absolute terms. No preferred mode in terms of t_s can thus be derived. This indicates that, once $\bar{E}$ (or rather Am) and $St_{D_{eq}}$ are within the feasible range that triggers the switching process, the switching time is a mere function of the jet speed. The average switching time at $Pr = 1.07$ amounts to $5.5\,ms$.

4.1.3 Dynamic Switching

Fig.9 a.) shows a forced oscillating jet at $f_{out} = 10\,Hz$ measured with the Pitot probe on side B. For each switching away from the measurement probe a significant undershoot is observed before the new steady state is reached. It is suggested that this is caused by the previously mentioned recirculation bubble that increases in size and elongates in the downstream direction. The undershoot is, in fact, a measure of the low pressure region inside the recirculation bubble that extends across the location of the Pitot probe. This is further supported by calculating the pressure difference across a reattached jet using the jet curvature equation as derived by Ries [31] and a jet centreline radius R equal to the attachment wall radius, so that

$$\Delta p = -\frac{\dot{m}^2}{\rho h^3 A R^2} \cdot \frac{1}{R} = -535\,Pa. \tag{6}$$

In general, the FSD can output any desired frequency pattern and is only limited by the minimum switching time t_s. Given the standard deviation of t_s of $\sigma = 9\%$ and that we defined the switching time as the time span between the onset of excitation and the point where 90% of the final mean value is reached, we can determine the maximum output oscillation frequency by:

$$f_{out}^{max} \leq \frac{0.9}{2 \cdot 1.09 \cdot t_{s,min}} = 75\,Hz \tag{7}$$

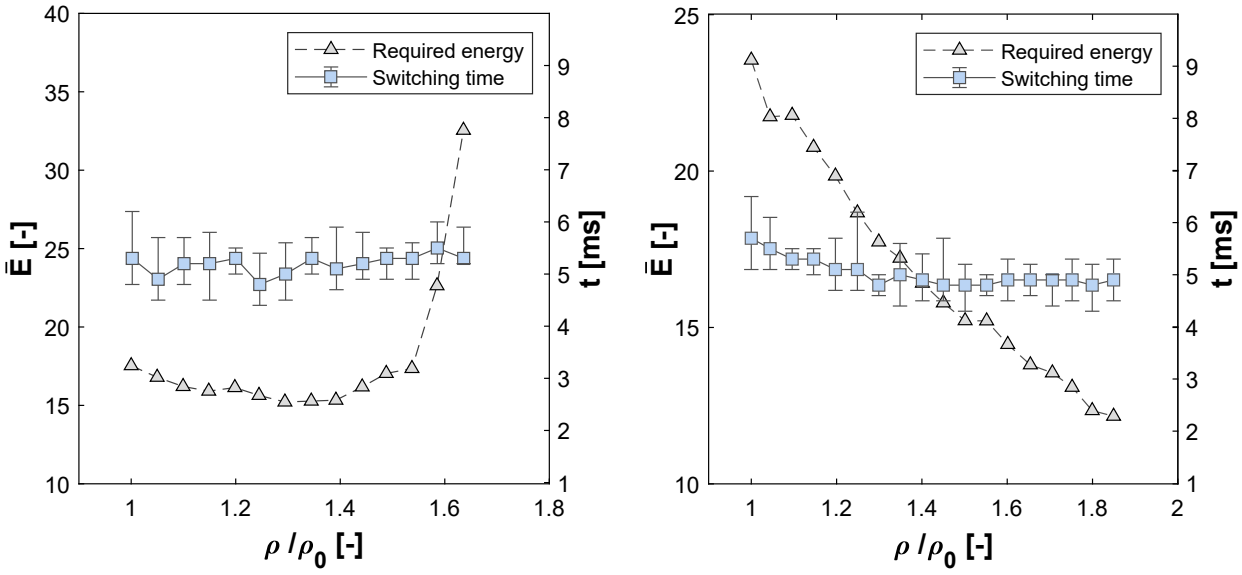

(a) $\hat{p} = const.$ (b) $Am = const.$

Fig. 10: Non-dimensional energy and absolute switching time vs. changes in density

Unfortunately, sometimes the switching process takes longer than $(1 + \sigma)t_{s,min}$ and so in practice the maximum reliable switching frequency was found to be $70\,Hz$ which corresponds to a 2σ deviation

$$f_{out}^{max} \leq \frac{0.9}{2 \cdot (1 + 2 \cdot \sigma) \cdot t_{s,min}} = 70\,Hz \tag{8}$$

Dynamic switching at $70\,Hz$ is displayed in Fig.9 b.).

4.1.4 Effect of Changes in Density

Temperature and absolute pressure in aerospace components differ from the conditions of typical bench test experiments. This is to say, the effect of changes in density on the behaviour of fluidic devices is crucial for the implementation in real world applications. Here the effect of changes in density is examined by increasing the mass flow rate while simultaneously adjusting the back pressure so as to maintain a constant volume flow rate. The pressure ratio across the device is therefore kept constant while the density increases. Fig.10 a.) shows the absolute

switching time along with the required non-dimensional energy as a function of $\frac{\rho}{\rho_0}$ at a constant pressure amplitude $\hat{p}$. The pressure amplitude is kept constant by decreasing the input voltage since $\hat{p}$ increases in compliance with the acoustic impedance ρc. The volume flow rate tested corresponds to a pressure ratio of $Pr = 1.07$ at $\frac{\rho}{\rho_0} = 1$. It can be seen that the required energy, in absolute and non-dimensional terms, increases exponentially as the density goes up. Since $\hat{p} = const$ and the increase in density is linear, it is the excitation time that has to be increased exponentially. However, at density ratios $\frac{\rho}{\rho_0} > 1.65$ an increase in excitation time is not able to cancel out the decrease in Am any more and switching becomes out of reach. The switching time t_s is somehow independent and is maintained around $5.5\,ms$. With a constant Amplitude Flow Factor Am Fig.10 b.) shows that the non-dimensional energy decreases linearly as the density goes up. This corresponds to a constant energy when put to absolute numbers ($\frac{Ap^2 t_{ex}}{\rho c} = const$). The switching time is again not affected. It is therefore concluded that the switching performance is independent of changes in density, and thus mass flow rate, if the Strouhal number $St_{D_{eq}}$ and the Amplitude Flow Factor Am remain constant. Moreover, since switching time is inversely related to the transport time, at same Mach number but hotter air the jet velocity will be faster and therefore switching time be shorter; in conjunction with independence of switching time to density this leads to conclude that there is no downside in performance when used at engine realistic conditions, i.e. high temperatures and high absolute pressures.

5 SUMMARY

We have presented an actively controlled bistable FSD that outputs any desired frequency pattern subject to the minimum switching time ($t_s = 5.5\,ms$). No additional air supply systems are needed and the switching mechanism relies entirely on the excitation of shear layer instabilities (See Part II for a more in-depth discussion on the respective shear layer instabilities). The operational bandwidth of the device goes up to pressure ratios around $PR = 1.14$ that yields Mach numbers up to $Mn \approx 0.3$. The acoustic signal was produced by standard, off the shelf and low cost ultrasonic transducers. The sound pressure level was amplified with an optimised control port geometry so that a 2D eigenmode matches the transducer resonance frequency. The absence of

a splitter not only reduces the complexity of the design but also demonstrates the ability to operate the device as a frequency controlled sweeping jet, a novelty with possible impact on applications like boundary layer separation control or unsteady film cooling. It was further suggested that the flow features a 'double attached' state after the excitation and prior to the point where the jet has fully switched.[1] While the increased entrainment has already achieved a pressure drop that causes the jet to detach and reattach to the opposite side the initial recirculation bubble persists for several flow through times while moving downstream causing a delay in switching. The introduction of a splitter could therefore considerably speed up the switching. Similar to the results presented in [38] it was shown that the sound pressure level has no significant effect on the switching as soon as a threshold is exceeded. Here the threshold for the non-dimensional amplitude at the preferred mode ($Pr \approx 1.14$) amounts to $Am = 0.11$. Furthermore it was shown that the switching performance does not decline at higher absolute pressures and densities. The discussion of the device performance based on non-dimensional parameters of geometry as well as signal properties serves as a guideline for future designs. The present concept of driving a bistable fluidic device with sound offers a promising alternative to conventional actuator technologies with the ability for closed-loop control.

ACKNOWLEDGMENTS

The authors would like to thank Rolls-Royce plc and the Engineering Physical Sciences Research Council (EP/L015196/1) for funding this work. The first author would also like to thank Chris Nicholls for all the discussions on fluidics.

NOMENCLATURE

A Area

AR Aspect ratio

c Speed of sound

D_{eq} Equivalent diameter of a circular jet

E Energy

[1] The corresponding flow field of the 'double attached' flow is shown in Part II

f Frequency

h Nozzle height

Mn Mach number

P Acoustic power

p Pressure

$\hat{p}$ Sound pressure

Pr Pressure ratio

Q Q-factor

Re Reynolds number

St Strouhal number

t Time

u_e Jet exit velocity

w Nozzle width

θ Momentum thickness

ρ Density

σ Standard deviation

LIST OF FIGURES

1 Left: Basic device layout and an example snapshot of a LES simulation showing attachment on side B. Right: Schematic and governing dimensions of the fluidic device in mm

2 Schematic of the experimental set-up

3 Cutaway model of the nozzle and interaction region and display of the acoustic domain

4 Acoustic optimisation of the control port chamber

5 Ten successive switching events measured via the Pitot probe (for location of probe see Fig.**??**) and close-up view for the comparison of different time scales

6 Non-dimensional switching parameters as a function of Pr

7 Non-dimensional and absolute switching time vs. Strouhal number and pressure ratio for different sound pressure levels

8 Schematic of a 'double attached' flow

9 Dynamic switching at two different oscillation frequencies

10 Non-dimensional energy and absolute switching time vs. changes in density

REFERENCES

[1] Cho, M., Choi, S., and Choi, H., 2016. "Control of flow separation in a turbulent boundary layer using time-periodic forcing". *ASME J. Fluids Eng.,* **138**(10), p. 101204.

[2] You, D., and Moin, P., 2008. "Active control of flow separation over an airfoil using synthetic jets". *Journal of Fluids and Structures,* **24**(8), pp. 1349–1357.

[3] Chapin, V., and Bénard, E., 2015. "Active control of a stalled airfoil through steady or unsteady actuation jets". *ASME J. Fluids Eng.,* **137**(9), p. 091103.

[4] Cerretelli, C., Wuerz, W., and Gharaibah, E., 2010. "Unsteady separation control on wind turbine blades using fluidic oscillators". *AIAA journal,* **48**(7), pp. 1302–1311.

[5] Koklu, M., 2018. "Effects of sweeping jet actuator parameters on flow separation control". *AIAA Journal*, pp. 100–110.

[6] Cerretelli, C., and Kirtley, K., 2009. "Boundary layer separation control with fluidic oscillators". *Journal of Turbomachinery,* **131**(4), p. 041001.

[7] Andino, M. Y., Lin, J. C., Washburn, A. E., Whalen, E. A., Graff, E. C., and Wygnanski, I. J., 2015. "Flow separation control on a full-scale vertical tail model using sweeping jet actuators". In 53rd AIAA Aerospace Sciences Meeting, p. 0785.

[8] Metka, M., and Gregory, J. W., 2015. "Drag reduction on the 25-deg ahmed model using fluidic oscillators". *ASME J. Fluids Eng.,* **137**(5), p. 051108.

[9] Seifert, A., Stalnov, O., Sperber, D., Arwatz, G., Palei, V., David, S., Dayan, I., and Fono, I., 2009. "Large trucks drag reduction using active flow control". In *The Aerodynamics of Heavy Vehicles II: Trucks, Buses, and Trains*. Springer, pp. 115–133.

[10] Woszidlo, R., Stumper, T., Nayeri, C., and Paschereit, C. O., 2014. "Experimental study

on bluff body drag reduction with fluidic oscillators". In 52nd Aerospace Sciences Meeting, p. 0403.

[11] Coulthard, S. M., Volino, R. J., and Flack, K. A., 2007. "Effect of jet pulsing on film cooling—part i: effectiveness and flow-field temperature results".

[12] Hossain, M. A., Prenter, R., Lundgreen, R. K., Ameri, A., Gregory, J. W., and Bons, J. P., 2018. "Experimental and numerical investigation of sweeping jet film cooling". *Journal of Turbomachinery,* **140**(3).

[13] Guyot, D., Bobusch, B., Paschereit, C. O., and Raghu, S., 2008. "Active combustion control using a fluidic oscillator for asymmetric fuel flow modulation". In 44th AIAA/ASME/SAE/ASEE Joint Propulsion Conference & Exhibit, p. 4956.

[14] Raman, G., Packiarajan, S., Papadopoulos, G., Weissman, C., and Raghu, S., 2005. "Jet thrust vectoring using a miniature fluidic oscillator". *The Aeronautical Journal,* **109**(1093), pp. 129–138.

[15] Parekh, D., Kibens, V., Glezer, A., Wiltse, J., and Smith, D., 1996. "Innovative jet flow control-mixing enhancement experiments". In 34th Aerospace Sciences Meeting and Exhibit, p. 308.

[16] Raman, G., and Cornelius, D., 1995. "Jet mixing control using excitation from miniature oscillating jets". *AIAA journal,* **33**(2), pp. 365–368.

[17] Raman, G., and Raghu, S., 2004. "Cavity resonance suppression using miniature fluidic oscillators". *AIAA journal,* **42**(12), pp. 2608–2612.

[18] Cattafesta III, L. N., Song, Q., Williams, D. R., Rowley, C. W., and Alvi, F. S., 2008. "Active control of flow-induced cavity oscillations". *Progress in Aerospace Sciences,* **44**(7-8), pp. 479–502.

[19] Lakebrink, M. T., Mani, M., and Winkler, C., 2017. "Numerical investigation of fluidic oscillator flow control in an s-duct diffuser". In 55th AIAA Aerospace Sciences Meeting, p. 1455.

[20] Gompertz, K., Pluim, J., and Bons, J., 2009. "Separation control authority of vortex generating jets in a low-pressure turbine with simulated wakes". In 47th AIAA Aerospace Sciences Meeting including The New Horizons Forum and Aerospace Exposition, p. 377.

[21] Fernandez, E., Kumar, R., and Alvi, F., 2013. "Separation control on a low-pressure turbine

blade using microjets". *Journal of propulsion and power,* **29**(4), pp. 867–881.

[22] Staats, M., and Nitsche, W., 2016. "Active control of the corner separation on a highly loaded compressor cascade with periodic nonsteady boundary conditions by means of fluidic actuators". *ASME J. of Turbomachinery,* **138**(3), p. 031004.

[23] Coleman, K., and McGee III, O., 2013. "Aeromechanical control of high-speed axial compressor stall and engine performance—part ii: Assessments of methodology". *ASME J. Fluids Eng.,* **135**(5), p. 051102.

[24] Tomac, M. N., and Gregory, J., 2012. "Frequency studies and scaling effects of jet interaction in a feedback-free fluidic oscillator". In 50th AIAA Aerospace Sciences Meeting including the New Horizons Forum and Aerospace Exposition, p. 1248.

[25] Tesař, V., Hung, C.-H., and Zimmerman, W. B., 2006. "No-moving-part hybrid-synthetic jet actuator". *Sensors and Actuators A: Physical,* **125**(2), pp. 159–169.

[26] Koklu, M., and Owens, L. R., 2017. "Comparison of sweeping jet actuators with different flow-control techniques for flow-separation control". *AIAA Journal,* **55**(3), pp. 848–860.

[27] Gregory, J., and Tomac, M. N., 2013. "A review of fluidic oscillator development". In 43rd AIAA Fluid Dynamics Conference, p. 2474.

[28] Raghu, S., 2013. "Fluidic oscillators for flow control". *Experiments in Fluids,* **54**(2), p. 1455.

[29] Foster, K., and Parker, G. A., 1970. *Fluidics: components and circuits*. John Wiley & Sons.

[30] Cattafesta III, L. N., and Sheplak, M., 2011. "Actuators for active flow control". *Annual Review of Fluid Mechanics,* **43**, pp. 247–272.

[31] Ries, J. P., 1972. Dynamic modeling of the bistable fluid amplifier. Tech. rep., Lehigh University.

[32] Joyce, J. W., 1983. Fluidics: basic components and applications. Tech. rep., Harry Doamond Labs.

[33] Gregory, J. W., Gnanamanickam, E. P., Sullivan, J. P., and Raghu, S., 2009. "Variable-frequency fluidic oscillator driven by a piezoelectric bender". *AIAA Journal,* **47**(11), pp. 2717–2725.

[34] Gregory, J., Ruotolo, J., Byerley, A., and McLaughlin, T., 2007. "Switching behavior of a

plasma-fluidic actuator". In 45th AIAA Aerospace Sciences Meeting and Exhibit, p. 785.

[35] Tesař, V., and Šonskỳ, J., 2015. "No-moving-part electro/fluidic transducer based on plasma discharge effect". *Sensors and Actuators A: Physical,* **232**, pp. 20–29.

[36] Martin, N. D., Bottomley, M., and Packwood, A., 2014. "Switching of a bistable diverter valve with synthetic jet actuators". *AIAA Journal,* **52**(7), pp. 1563–1568.

[37] Chen, L.-W., Turner, J., Bacic, M., and Ireland, P., 2016. "Exeprimental and numerical studies of a plasma fluidic device for active flow control". In 8th AIAA Flow Control Conference, p. 4235.

[38] Mair, M., Bacic, M., and Ireland, P., 2019. "On dynamics of acoustically driven bistable fluidic valves". *Journal of Fluids Engineering,* **141**(6).

[39] Roger, R., and Chan, S., 2003. "Numerical study of fluidic bistable amplifiers". In 33rd AIAA fluid dynamics conference and exhibit, p. 3459.

[40] Tam, C. K., 1978. "Excitation of instability waves in a two-dimensional shear layer by sound". *Journal of Fluid Mechanics,* **89**(2), pp. 357–371.

[41] Garnaud, X., Lesshafft, L., Schmid, P., and Huerre, P., 2013. "The preferred mode of incompressible jets: linear frequency response analysis". *Journal of Fluid Mechanics,* **716**, pp. 189–202.